

¹ Southern Ocean Water Mass Transformation Driven by ² Sea Ice

³ Ryan P. Abernathey^{1*}, Ivana Cerovecki⁴, Paul R. Holland², Emily Newsom³, Matt Mazloff⁴, and

⁴ Lynne D. Talley⁴

⁵ ¹*Lamont Doherty Earth Observatory of Columbia University, Palisades, New York, USA*

⁶ ²*British Antarctic Survey, Cambridge, UK.*

⁷ ³*University of Washington, Seattle, Washington, USA*

⁸ ⁴*Scripps Institution of Oceanography, La Jolla California, USA*

⁹ **A major question for the global ocean circulation is how dense abyssal waters regain buoy-**
¹⁰ **ancy and return to the surface¹. The steeply sloping isopycnals of the Southern Ocean pro-**
¹¹ **vide a pathway for Circumpolar Deep Water (CDW) to upwell without mixing^{2–4}. Once near**
¹² **the surface, CDW is transformed directly by surface fluxes, splitting into an upper and lower**
¹³ **circulation branch^{5–7}. It has been postulated that sea ice contributes to these fluxes^{8–11}, but its**
¹⁴ **relative importance is largely unknown due to a paucity of observations of sea ice thickness**
¹⁵ **and transport^{12,13}. Here we quantify the sea ice freshwater flux using the Southern Ocean**
¹⁶ **State Estimate, a state-of-the-art data assimilation that incorporates millions of ocean and**
¹⁷ **ice observations. Sea ice dominates surface freshwater exchange compared to precipitation**
¹⁸ **and glacial ice melt, with melt fluxes exceeding $0.5 \times 10^6 \text{ m}^3 \text{ s}^{-1}$. The water mass transfor-**
¹⁹ **mation framework¹⁴ reveals that brine rejection and ice melt fluxes are the main processes**
²⁰ **responsible for destroying upwelling CDW, at a rate of $\sim 22 \times 10^6 \text{ m}^3 \text{ s}^{-1}$. These results**

21 imply a prominent role for Antarctic sea ice in the global ocean circulation and suggest that,
22 as Antarctic sea ice evolves with climate change, the ocean's overturning circulation may be
23 affected.

24 The Southern Ocean State Estimate (SOSE) is an ice/ocean data assimilation produced for
25 the time period Jan. 2005 through Dec. 2010. (See Methods and Supplementary Information for
26 SOSE details and validation.) The bulk freshwater fluxes at the ocean surface south of 50° S, as
27 estimated by SOSE, are summarized in Fig. 1a. When sea ice forms, nearly all of the salt remains
28 behind in the underlying seawater (a process called “brine rejection”); when the ice melts, liquid
29 freshwater is returned to the ocean. Direct open-ocean precipitation minus evaporation (0.28 Sv)
30 and glacial ice melt (0.05 Sv) are both smaller than net sea ice melt (0.50 Sv) and brine rejection
31 (0.36 Sv). ($1 \text{ Sv} = 10^6 \text{ m}^{-3} \text{ s}^{-1} \simeq 3.15 \times 10^4 \text{ Gt freshwater / year}$.) Melt exceeds brine rejection
32 because sea ice incorporates snowfall at a rate of 0.14 Sv. Moreover, wind-driven sea ice transport
33 creates a freshwater conveyor belt from the Antarctic coast to the open ocean¹⁵, leading to sharp
34 gradients in freshwater flux. The spatial structure of the sea-ice redistribution is assessed in Fig. 1b
35 by comparing the annual mean freshwater flux leaving the atmosphere, land, and glaciers (left
36 panel) with that entering the ocean (right panel); the difference is due to sea ice freshwater redistri-
37 bution (middle panel, vectors show the ice thickness transport). From the atmosphere, widespread
38 precipitation over the Southern Ocean leads to a broadly distributed positive freshwater flux with a
39 characteristic magnitude of 0.5 m / year, and glacial ice melt provides a stronger freshwater source
40 near the Antarctic coast. (SOSE does not include subsurface ice shelf fluxes.) Sea ice reverses
41 the sign of the freshwater flux near the coast, through both brine rejection and snow interception.

42 Ice is transported away from Antarctica and melted near the Southern Front of the Antarctic Cir-
43 cumpolar Current, where the melt flux greatly exceeds the precipitation rate. As a result, the net
44 freshwater flux to the ocean closely resembles the sea-ice redistribution flux, with much stronger
45 gradients than the atmospheric fluxes alone could produce. Fig. 1c shows the freshwater transport
46 by atmosphere and sea ice averaged in ocean surface neutral density coordinates, revealing that ice
47 process systematically transport freshwater from CDW to Antarctic Intermediate Water (AAIW)
48 and Subantarctic Mode Water (SAMW) classes at a rate of nearly 0.2 Sv. The atmospheric trans-
49 port (0.5 Sv) is in the opposite direction and, while larger overall, acts over a much broader density
50 range. The large sea ice freshwater fluxes have a major impact on the density of seawater, and
51 consequently, the stratification and circulation of the Southern Ocean.

52 The importance of sea ice formation for the production of High Salinity Shelf Water, and
53 eventually Antarctic Bottom Water (AABW), is widely accepted¹⁶. Modeling studies have shown
54 a relationship between lateral transport of Antarctic sea ice and the strength of the AABW cell^{8–10},
55 and it has therefore been hypothesized that expanded Antarctic sea ice during the last glacial pe-
56 riod was accompanied by a more vigorous AABW overturning circulation^{17,18}. Model experiments
57 have also shown that the excess freshwater exported via sea ice to the open Southern Ocean con-
58 tributes to the production of fresh Antarctic Intermediate Water (AAIW) and therefore helps sus-
59 tain the upper branch of the overturning¹¹. It has further been argued that the buoyancy gain in
60 upwelling CDW comes primarily from freshwater fluxes, not heat fluxes¹⁹.

61 To quantify the impact of sea ice processes on the overturning circulation, we apply the

62 water mass transformation framework¹⁴ to brine rejection and ice melt. The transformation rate
63 quantifies the rate at which a given water mass is made lighter (negative transformation rate) or
64 denser (positive) due to diabatic processes, i.e. surface fluxes and mixing. (See Methods and
65 Supplementary Information for details of the calculation.) Averaged over a basin, it represents
66 the net volume flux across an isopycnal surface. If this volume flux is not constant in the upper
67 ocean over a given density range, it implies that water must be subducted to or upwelled from
68 the interior in that range order to satisfy mass continuity²⁰, providing a quantitative link between
69 between surface thermodynamic processes and overturning circulation. A few past studies have
70 calculated the transformation rate due to ocean-ice freshwater exchange as part of more general
71 analysis of model simulations^{19,21}. Here we apply this approach within SOSE, thereby leveraging
72 nearly all available observational data from the Southern Ocean from 2005-2010.

73 First we consider the transformation induced by the surface air-ice-ocean fluxes, plotted in
74 Fig. 2a. The net surface transformation (solid black) is the sum of heat-flux-induced transformation
75 (red) and freshwater-flux-induced transformation (blue). In agreement with other studies, fresh-
76 water fluxes dominate the surface transformation in the high-latitude Southern Ocean^{19,22}. The
77 freshwater-driven transformation is characterized by a broad region of strongly negative transfor-
78 mation (i.e. buoyancy gain) in the density range $26.6 < \gamma_n < 27.6 \text{ kg m}^{-3}$, peaking at more than 25
79 Sv, and a region of positive transformation (buoyancy loss) at higher densities ($\gamma_n > 27.6 \text{ kg m}^{-3}$).
80 The freshwater transformation can be further decomposed into contributions from direct exchange
81 with the atmosphere, land, and terrestrial ice (evaporation, precipitation, and runoff / glacial ice
82 melt; green), brine rejection from freezing sea ice (purple), and freshwater from melting ice (or-

83 ange). Freezing and melting both contribute strongly, and in opposite senses (approx. ± 20 Sv),
84 to the transformation but do so over different density ranges. The positive peak in net freshwater-
85 induced transformation near $\gamma_n = 27.7 \text{ kg m}^{-3}$ can clearly be attributed to brine rejection, and the
86 transformation due to melting sea ice is larger than that due to precipitation, demonstrating that
87 sea-ice freshwater fluxes make a first-order contribution to Southern Ocean water mass transfor-
88 mation. It is particularly noteworthy that the freshwater transport of order 0.2 Sv (Fig. 1c) drives
89 transformation rates 100 times larger.

90 The difference between the transformation that *would have* occurred if all the precipitation
91 passed directly to the ocean (dashed green) and the actual transformation (solid green) can be
92 attributed to sea-ice freshwater redistribution (dashed blue). This curve highlights how sea-ice
93 freshwater redistribution drives water mass divergence in density space at a rate of over 20 Sv.
94 The difference dashed green and solid green represents the effect of snow interception by sea ice,
95 which weakens transformation by up to 10 Sv in the UCDW range.

96 Upper ocean mixing and mixed-layer entrainment also contribute significantly to water mass
97 transformation^{20,23}. Because sea ice growth, brine rejection, and vertical mixing have a tightly
98 coupled relationship in the Southern Ocean^{24,25}, mixing-induced transformation must be consid-
99 ered together with the surface fluxes. Fig. 2b shows the transformation due to vertical (solid) and
100 horizontal (dashed) mixing of heat (red) and salt (blue) in the upper 670 m (a depth which encom-
101 passes most of the seasonal mixed layer). Mixing is weaker overall than surface transformation.
102 As in previous studies, vertical mixing of salt is the dominant term¹⁹. The net mixing-induced

103 transformation (black) is clearly homogenizing in nature, acting to densify water of $\gamma_n < 27.5$
104 kg m^{-3} and lighten water above this value. The net upper-ocean transformation rate, comprising
105 both surface fluxes and mixing, is shown in Fig. 2a as the thick dashed line. Downward mixing of
106 freshwater from AAIW densities counteracts the positive transformation caused by surface fluxes
107 (mostly brine rejection) in the UCDW range.

108 In Fig. 2c, we plot the formation rate, integrated in 0.1 kg m^{-3} density bins, for a select
109 combination of components. The formation rate is the derivative of the transformation rate with
110 respect to density. It represents the volume convergence in density space—negative formation
111 (i.e. destruction) in the upper ocean over a particular density range indicates that water in that
112 range must be upwelled from the ocean interior. Examining first the net formation (black), we see
113 a strong destruction of water in the range $27.3 < \gamma_n < 27.8 \text{ kg m}^{-3}$. Encompassing much of the
114 UCDW densities and also denser AAIW, this clearly corresponds with the upwelling branch of the
115 MOC and the Antarctic divergence. The combined effects of ice freezing and melt (purple) make
116 the dominant contribution to this destruction, with precipitation (green) in second place. These
117 processes are partially offset by heat fluxes (red) and mixing (dashed blue), which instead drive
118 formation in this range. At lower densities ($\gamma_n < 27.0 \text{ kg m}^{-3}$), strong formation is evident in the
119 Subantarctic Mode Water (SAMW) range, driven by both heat and freshwater fluxes. In contrast
120 with previous analysis which showed separate Indian and Pacific peaks in SAMW formation²⁶,
121 the SAMW formation here is more broadly distributed due to interannual variability in the Pa-
122 cific SAMW over the longer averaging period. At higher densities, heat fluxes drive formation
123 of AABW, with considerable opposition from vertical mixing. However, due to the lack of as-

¹²⁴ similated surface data for these densities, as well as the spurious nature of AABW production in
¹²⁵ SOSE, we consider the transformation and formation rates for $\sigma_\theta > 28.0 \text{ kg m}^{-3}$ unreliable; they
¹²⁶ are too low compared to estimates from inverse modeling^{5,7,16}. (See Supplementary Information
¹²⁷ for model validation and related discussion.)

¹²⁸ While the time-mean transformation rates presented above are what matter for net subduc-
¹²⁹ tion and upwelling, examining the seasonal variability in transformation is enlightening. In Fig. 3
¹³⁰ we plot the temporal variability over the six-year SOSE period of the dominant freshwater transfor-
¹³¹ mation components: direct evaporation/precipitation/runoff/glacial ice melt (top), sea ice freezing
¹³² and melt (middle), and the vertical mixing of salinity (bottom). This figure also shows sea-ice
¹³³ concentration averaged in density space, highlighting the relation between transformation and ice
¹³⁴ cover. The seasonal cycle in precipitation is clearly present but not particularly strong. In contrast,
¹³⁵ ice freezing and melt are extremely seasonal and correlated with the growth of ice cover. Partic-
¹³⁶ ularly striking is the fact that melt fluxes reach deep into SAMW and thermocline water²⁷. The
¹³⁷ mixing is also strongly seasonal, taking place mostly in summer and fall. Together with the surface
¹³⁸ fluxes, the temporal variability is indicative of the creation of a shallow, fresh summer mixed layer
¹³⁹ following ice melt, which is subsequently eroded by vertical mixing through the fall as ice re-
¹⁴⁰ forms, consistent with simple models and under-ice observations^{24,25,28}. The intricate, temporally
¹⁴¹ variable relationship between ice formation, freshwater fluxes, and mixing highlights the need for
¹⁴² year-round data in order to accurately quantify the water mass transformation driven by sea ice
¹⁴³ processes.

144 Trends in sea ice concentration have received much attention as a proxy for polar climate
145 change²⁹. From the ocean's perspective, however, it is sea ice freshwater *transport*, rather than
146 *extent*, which matters most. SOSE's six-year time period does not allow us to examine the decadal
147 trends in water mass transformation directly; however, our results suggest that recent wind-driven
148 trends in Antarctic sea ice transport¹⁵ should be associated with changes in water mass transforma-
149 tion. It was recently proposed that these trends over the past 30 years, and the accompanying fresh-
150 water flux anomalies, can mostly explain decadal trends in Southern Ocean salinity³⁰. Our trans-
151 formation calculations imply that, if wind-driven sea-ice export increases, CDW will be destroyed
152 at a faster rate, potentially accelerating the overturning circulation. Enhancing our knowledge of
153 Antarctic sea ice thickness and transport, the under-ice mixing process, and the atmospheric and
154 oceanic drivers of ice transport variability through increased year-round observations should be a
155 fruitful direction for deepening our understanding of the global ocean overturning system.

156 Methods

157 **Southern Ocean State Estimate** Sparse observations are a major obstacle to accurate characteri-
158 zation of Southern Ocean physics. Current Antarctic sea ice thickness and velocity measurements
159 do not provide sufficient spatial and temporal resolution for an observationally derived budget; nev-
160 ertheless there have been a few attempts to estimate the seasonal freshwater fluxes associated with
161 sea ice growth and melt from the limited observations^{12,13,30}. All these studies have showed that
162 sea-ice induced freshwater fluxes are large compared to typical precipitation rates. In addition to
163 ice data, the water mass transformation calculation further requires knowledge of the time-varying

¹⁶⁴ correlation between surface fluxes and the underlying water temperature and salinity. Given these
¹⁶⁵ challenges, our approach here is to use a highly realistic, carefully validated data-assimilating nu-
¹⁶⁶ merical model to examine the effects of sea-ice processes on Southern Ocean water masses.

¹⁶⁷ We employ SOSE iteration 100, a high-resolution general circulation model that has been
¹⁶⁸ constrained, via an adjoint method, to nearly all available observations, including sea ice concen-
¹⁶⁹ tration, in the 2005-2010 period. This approach provides an optimal synthesis of the observations
¹⁷⁰ that is also consistent with known physical and thermodynamic constraints. Crucially, SOSE in-
¹⁷¹ cludes a dynamic sea ice model which shows good agreement with observed sea ice thickness,
¹⁷² concentration, and velocity data, suggesting it can provide an accurate estimate of the freshwater
¹⁷³ budget. The resolution of SOSE ($1/6^\circ$) is eddy permitting, and vigorous mesoscale motions are
¹⁷⁴ present in the solution. A technical description of SOSE and comprehensive validation its sea ice
¹⁷⁵ and hydrography can be found in Supplementary Information. This validation indicates that SOSE
¹⁷⁶ agrees very well with observations in the SAMW, AAIW, and UCDW range, which are the primary
¹⁷⁷ focus of this study.

¹⁷⁸ As with many numerical models, the net production of AABW ($\gamma_n > 28.2 \text{ kg m}^{-3}$) is unreal-
¹⁷⁹ istically weak in SOSE, probably due to poor representation of coastal polynyas. Furthermore, all
¹⁸⁰ of this production occurs in the first year and is not sustained. (Further details are given in Supple-
¹⁸¹ mentary Information.) This shortcoming, together with SOSE's lack of a freshwater source from
¹⁸² subsurface glacial melt and the overall paucity of assimilation data in this density range, means
¹⁸³ that we have low confidence in the transformation rates for AABW.

¹⁸⁴ **Water Mass Transformation** Transformation is calculated as

$$\Omega(\sigma, t) = \frac{\partial}{\partial \sigma} \int_{\sigma' < \sigma} \left(\frac{\partial \sigma}{\partial \theta} \dot{\theta} + \frac{\partial \sigma}{\partial S} \dot{S} \right) dV \quad (1)$$

¹⁸⁵ where σ is potential density, t is time, and $\dot{\theta}$ and \dot{S} represent all non-advection sources (i.e. external
¹⁸⁶ forcing and mixing) of potential temperature (θ) and salinity (S), respectively. The transformation
¹⁸⁷ rate Ω can be linearly decomposed into many different contributions from different processes, and
¹⁸⁸ the volume integral reduces to a surface integral for surface fluxes. (The technical details of the
¹⁸⁹ calculation are described in Supplementary Information.)

¹⁹⁰ Since this study is concerned with upper-ocean processes, we calculate transformation with
¹⁹¹ respect to surface-referenced potential density (σ_θ); however, we label our plots with neutral den-
¹⁹² sity (γ_n) in order to best identify well-known water masses. (See Supplementary Information for
¹⁹³ details of relabeling procedure.) We focus on the density range $\gamma_n > 26.0$. We define Thermocline
¹⁹⁴ Water (TW; $\gamma_n < 26.6 \text{ kg m}^{-3}$), Subantarctic Mode Water (SAMW; $26.6 < \gamma_n < 27.0 \text{ kg m}^{-3}$),
¹⁹⁵ Antarctic Intermediate Water (AAIW; $27.0 < \gamma_n < 27.5 \text{ kg m}^{-3}$), Upper Circumpolar Deep Water
¹⁹⁶ (UCDW; $27.5 < \gamma_n < 28.0 \text{ kg m}^{-3}$), Lower Circumpolar Deep Water (LCDW; $28.0 < \gamma_n < 28.2$
¹⁹⁷ kg m^{-3}), and Antarctic Bottom Water (AABW; $\gamma_n > 28.2 \text{ kg m}^{-3}$), following previous studies^{5,22}.

¹⁹⁸ 1. Ferrari, R. What goes down must come up. *Nature* **513**, 179–180 (2014).

²⁰⁰ 2. Toggweiler, R. & Samuels, B. Effect of Drake Passage on the global thermohaline circulation.
²⁰¹ *Deep Sea Res. I* **42**, 477–500 (1995).

- 202 3. Wolfe, C. & Cessi, P. The adiabatic pole-to-pole overturning circulation. *J. Phys. Oceanogr.*
- 203 **41**, 1795–1810 (2011).
- 204 4. Nikurashin, M. & Vallis, G. A theory of the interhemispheric meridional overturning circula-
- 205 tion and associated stratification. *J. Phys. Oceanogr.* **42**, 1652–1667 (2012).
- 206 5. Speer, K., Rintoul, S. & Sloyan, B. The diabatic Deacon cell. *J. Phys. Oceanogr.* **30**, 3212–
- 207 3223 (2000).
- 208 6. Marshall, J. & Speer, K. Closing the meridional overturning circulation through Southern
- 209 Ocean upwelling. *Nature Geoscience* **5**, 171–180 (2012).
- 210 7. Talley, L. D. Closure of the global overturning circulation through the Indian, Pacific and
- 211 Southern Oceans: schematics and transports. *Oceanography* **26**, 80–97 (2013).
- 212 8. Hasumi, H. & Sugino, N. Haline circulation induced by formation and melting of sea ice.
- 213 *J. Geophys. Res.* **100**, 20,613–20,625 (1995).
- 214 9. Stoessel, A., Kim, S. & Drijfhout, S. B. The impact of Southern Ocean sea ice in a global
- 215 ocean model. *J. Phys. Oceanogr.* **28**, 1999–2018 (1998).
- 216 10. Komuro, Y. & Hasumi, H. Effects of surface freshwater flux induced by sea ice transport on
- 217 the global thermohaline circulation. *J. Geophys. Res.* **108**, 3047 (2003).
- 218 11. Saenko, O. A., Schmittner, A. & Weaver, A. J. On the role of wind-driven sea ice motion on
- 219 ocean ventilation. *J. Phys. Oceanogr.* **32**, 3376–3395 (2002).

- 220 12. Ren, L., Speer, K. & Chassignet, E. P. The mixed layer salinity budget and sea ice in the
221 Southern Ocean. *J. Geophys. Res.* **116**, C08031 (2011).
- 222 13. Tamura, T., Ohshima, K. I., Nihashi, S. & Hasumi, H. Estimation of surface heat/salt fluxes
223 associated with sea ice growth/melt in the southern ocean. *Sci. Online Lett. on the Atmos.* **7**,
224 17–20 (2011).
- 225 14. Walin, G. On the relation between sea-surface heat flow and thermal circulation in the ocean.
226 *Tellus* **34**, 187–195 (1982).
- 227 15. Holland, P. R. & Kwok, R. Wind-driven trends in Antarctic sea-ice drift. *Nature Geoscience*
228 **5**, 872–875 (2012).
- 229 16. Jacobs, S. Bottom water production and its links with the thermohaline circulation. *Antarctic*
230 *Science* **4** (2004).
- 231 17. Stephens, B. B. & Keeling, R. F. The influence of antarctic sea ice on glacial–interglacial CO₂
232 variations. *Nature* **404**, 171–174 (2000).
- 233 18. Ferrari, R. *et al.* Antarctic sea ice control on ocean circulation in present and glacial climates.
234 *Proc. Natl. Acad. Sci.* **111**, 8753–8758 (2014).
- 235 19. Iudicone, D., Madec, G., Blanke, B. & Speich, S. The role of southern ocean surface forcings
236 and mixing in the global conveyor. *J. Phys. Oceanogr.* **38** (2008).
- 237 20. Marshall, J., Jamous, D. & Nilsson, J. Reconciling thermodynamic and dynamic methods of
238 computation of water-mass transformation rates. *Deep Sea Res. I* **46**, 545–572 (1999).

- 239 21. Urakawa, L. & Hasumi, H. Eddy-resolving model estimate of the cabling effect on the water
240 mass transformation in the Southern Ocean. *J. Phys. Oceanogr.* **42**, 1288–1302 (2012).
- 241 22. Downes, S. M., Gnanadesikan, A., Griffies, S. M. & Sarmiento, J. L. Water mass exchange in
242 the Southern Ocean in coupled climate model. *J. Phys. Oceanogr.* **41**, 1756–1771 (2011).
- 243 23. Garrett, C. & Tandon, A. The effects on water mass formation of surface mixed layer time-
244 dependence and entrainment fluxes. *Deep Sea Res. I* **44**, 1991–2006 (1997).
- 245 24. Gordon, A. L. & Huber, B. A. Southern Ocean winter mixed layer. *J. Geophys. Res.* **95**,
246 11,544–11,672 (1990).
- 247 25. Martinson, D. Evolution of the Southern Ocean winter mixed layer and sea ice: Open ocean
248 deepwater formation and ventilation. *J. Geophys. Res.* **95**, 11,641–11,654 (1990).
- 249 26. Cerovečki, I., Talley, L. D. & Mazloff, M. Subantarctic mode water formation, destruction,
250 and export in the eddy-permitting Southern Ocean State Estimate. *J. Phys. Oceanogr.* **42**,
251 1485–1511 (2012).
- 252 27. Cerovečki, I. & Mazloff, M. R. The spatiotemporal structure of diabatic processes governing
253 the evolution of subantarctic mode water in the southern ocean. *Journal of Physical Oceanog-
254 raphy* (2015).
- 255 28. Wong, A. P. S. & Riser, S. C. Profiling float observations of the upper ocean under sea ice off
256 the Wilkes Land coast of Antarctica. *J. Phys. Oceanogr.* **41**, 1102–1115 (2011).

257 29. Cavalieri, D., Parkinson, C. & Vinnikov, K. Y. 30-year satellite record reveals contrasting

258 Arctic and Antarctic decadal sea ice variability. *Geophysical Research Letters* **30** (2003).

259 30. Haumann, F. A., Gruber, N., Muennich, M., Frenger, I. & Kern, S. Sea-ice transport driving

260 southern ocean salinity and its recent trends (2015). In review at Nature.

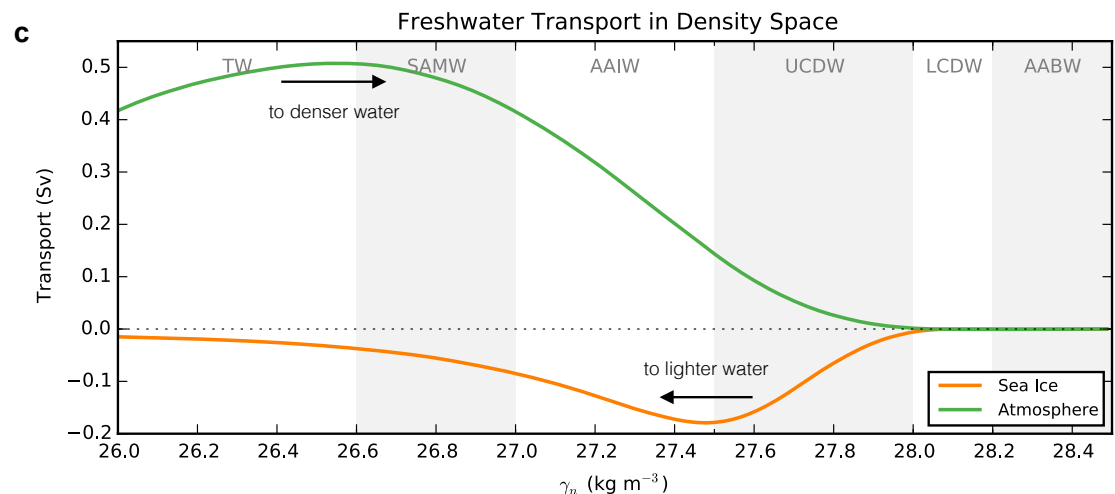
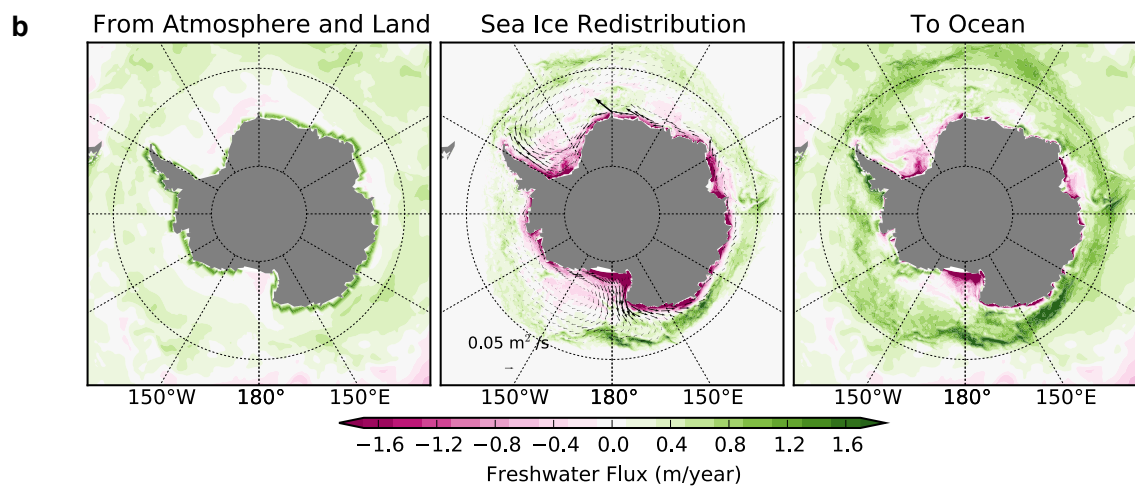
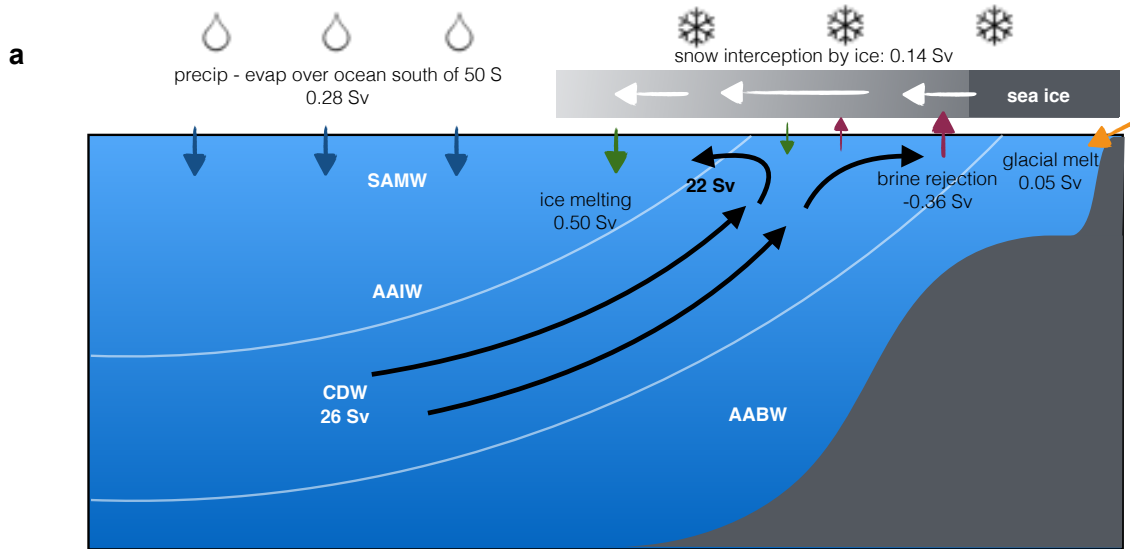
261 **Acknowledgements** R.P.A. acknowledges support from NSF grant OCE-1357133. I.C., L.D.T., and

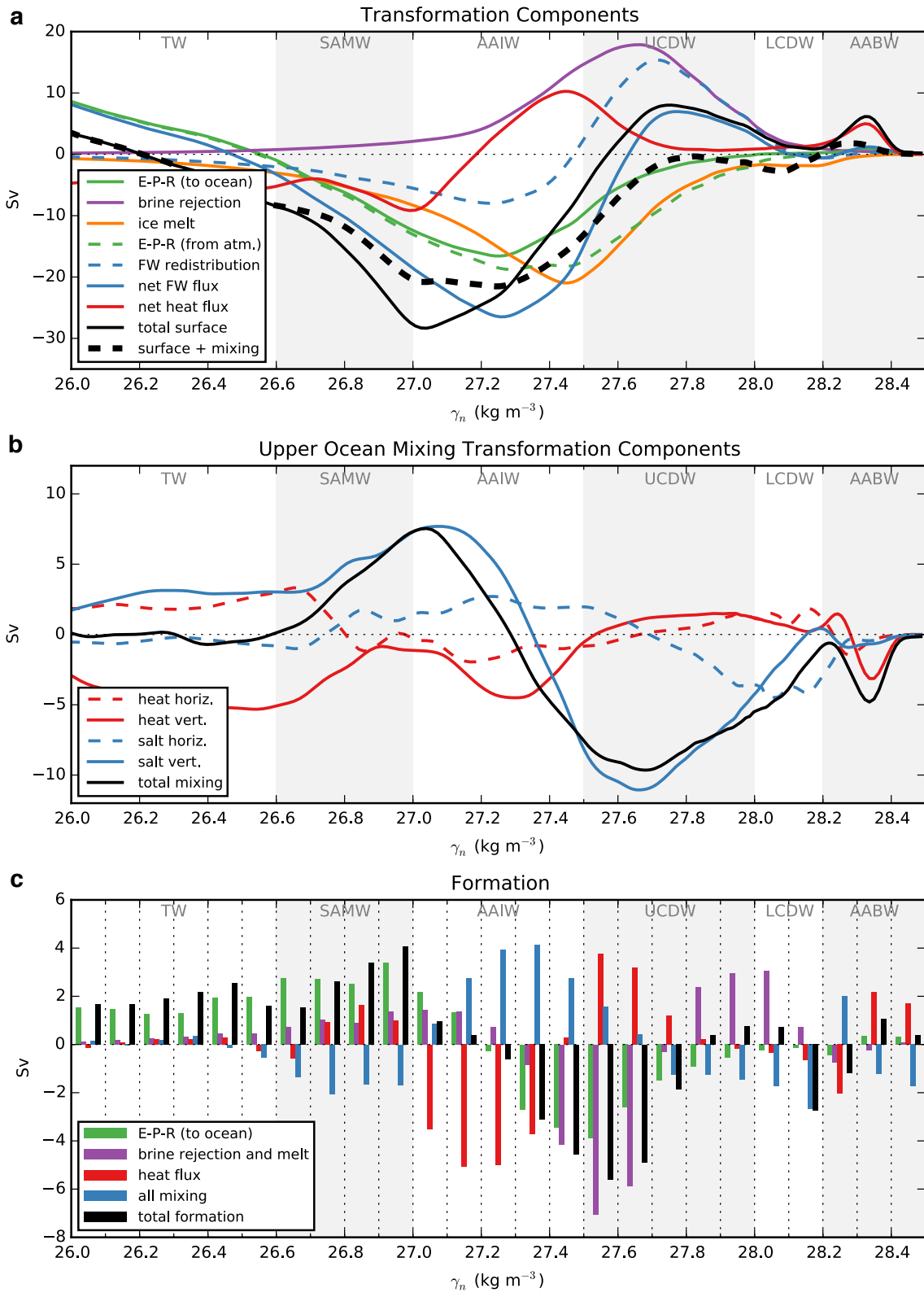
262 M.M. acknowledge support from NSF grant OCE-1357072. L.T. acknowledges additional support from

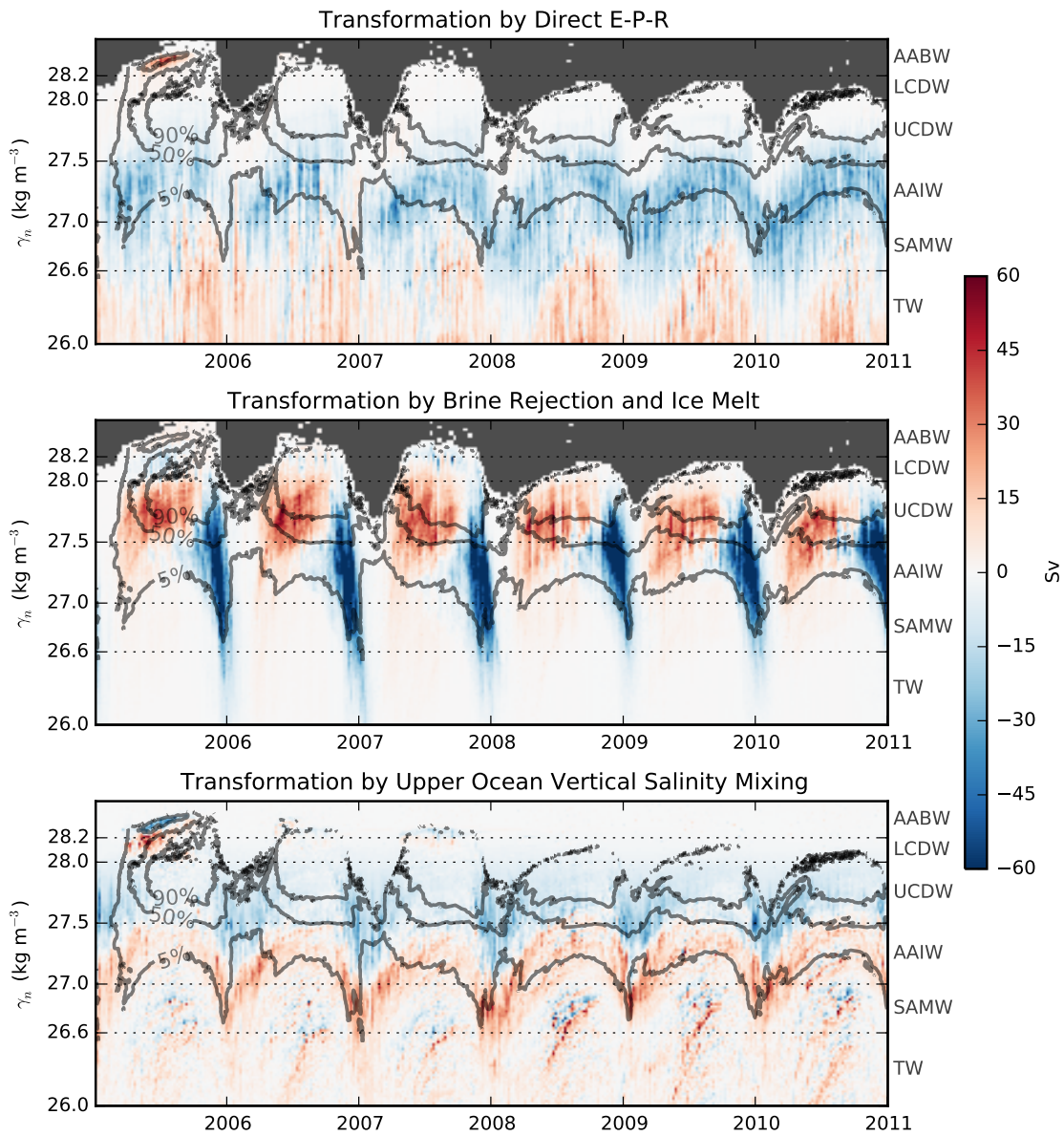
263 NSF grant PLR-1425989.

264 **Competing Interests** The authors declare that they have no competing financial interests.

265 **Correspondence** Correspondence and requests for materials should be addressed to R.P.A. (rpa@ldeo.columbia.edu).







269 **Figure 1** a) Schematic depicting the various bulk contributions to the freshwater flux
270 at the ocean surface. b) Annual mean freshwater fluxes from for the period 2005-2011.
271 Left panel shows the flux leaving the atmosphere and land, and right panel shows the
272 flux entering the ocean. Center panel shows the sea ice redistribution flux (the difference
273 between the two), with arrows indicating the lateral sea ice thickness transport. c) Lat-
274 eral freshwater transport by atmosphere and sea ice, averaged in ocean surface density
275 coordinates.

276 **Figure 2** a) Water mass transformation due to surface fluxes. The net upper-ocean
277 transformation (including mixing) is given by the thick dashed line. E-P-R mean evapora-
278 tion minus precipitation minus runoff (including glacial ice melt). b) Contribution of mixing
279 processes to transformation in the 670 m. c) Corresponding formation rates, integrated in
280 0.1 kg m^{-3} bins.

281 **Figure 3** Timeseries of freshwater transformation over the six year state estimate, as a
282 function of time (x-axis) and potential density (y-axis). a) Surface transformation due to
283 direct freshwater exchange with the atmosphere (evaporation minus precipitation). The
284 gray mask indicates isopycnals that outcrop neither under air nor ice, and the gray con-
285 tours show the density-averaged sea ice concentration (contours at 5%, 50% and 90%).
286 b) Surface transformation due to ice freezing and melting. c) Transformation due to mixing
287 of salinity in the upper 670 m.